Mathematical Biosciences and Engineering, 16(3): 1067–1081.
DOI: 10.3934/mbe.2019051
Received: 06 December 2018
Accepted: 01 January 2019
Published: 15 February 2019

http://www.aimspress.com/journal/MBE

Research article

A fast 3-D ultrasound projection imaging method for scoliosis assessment

Wei-wei Jiang[1], Guang-quan Zhou[2,*], Ka-Lee Lai[3], Song-yu Hu[4], Qing-yu Gao[1], Xiao-yan Wang[1] and Yong-ping Zheng[3,*]

[1] College of Computer Science & Technology, Zhejiang University of Technology, Hangzhou, China
[2] State Key Laboratory of Bioelectronics, School of Biological Science and Medical Engineering, Southeast University, Nanjing, China
[3] Interdisciplinary Division of Biomedical Engineering, The Hong Kong Polytechnic University, Kowloon, Hong Kong, China
[4] College of Mechatronics and Control Engineering, Shenzhen University, Shenzhen, China

* **Correspondence:** Email: guangquan.zhou@seu.edu.cn, ypzheng@ieee.org; Tel: +862583792246, +85227667664; Fax: +85223342429.

Abstract: Applying ultrasound for scoliosis assessment has been an attractive topic over the past decade. This study proposed a new fast 3-D ultrasound projection imaging method to evaluate the spine deformity. A narrow-band rendering method was used to generate the coronal images based on B-mode images and their corresponding positional data. The non-planar reslicing method, which followed the natural spine curve, was used to project the complete spine data into the coronal image. The repeatability of the new method was tested. A comparison experiment on the reconstructed images and the processing time between the conventional 3-D rendering method and the developed projection imaging method was also performed among 70 patients with scoliosis. The intra- and inter-operator tests results demonstrated very good repeatability (ICC $\geq$ 0.90). The mean processing times for the developed projection method and conventional rendering method were 15.07 $\pm$ 0.03 s and 130.31 $\pm$ 35.07 s, respectively. The angle measurement results showed a high correlation ($y = 0.984x$, $r = 0.954$) between the images obtained using the two methods. The above results indicated that the developed projection imaging method could greatly decrease the processing time while preserving the comparative image quality. It can be expected that this novel method may help to provide fast 3-D ultrasound diagnosis of scoliosis in clinics.

Keywords: 3-D rendering; scoliosis assessment; ultrasound; fast imaging; clinical trial

1. Introduction

Scoliosis is a medical condition defined as a 3-D spine deformity with the lateral deviation and the vertebral axial rotation [1,2]. Over 65% scoliosis is the Adolescent idiopathic scoliosis (AIS), affecting the 3.08% of the population in Hong Kong [3], 2% to 4% in the United States [4], and 5.2% in Germany [5]. Long term studies presented that scoliosis could inevitably lead to a series of health problems, including the spine degeneration [6], back pain [7,8], thoracic insufficiency syndrome [9], and psychosocial issues such as lowered self-image and increased depression [10]. The exact etiology of AIS is still unknown [11], though many risks of curve progression, including the curve pattern, Cobb angle, Risser sign, sitting and standing heights, have been reported [12–14]. In clinics, up to now, the diagnosis method has been limited to regular monitoring [15], which is also essential for the follow-up diagnosis, evaluation and treatment [16]. According to the diagnosis results, different treatment methods, including physical therapy, brace treatment, and surgery, can be applied to different types of AIS patients [17–20].

The gold standard for scoliosis curvature assessment is the Cobb angle measurement on the standing X-ray radiograph [21]. To monitor the curve progression or evaluate the treatment outcome, regular X-ray examination is usually performed in clinics [15]. However, frequent exposure to X-ray may increase the risk of breast cancer for girls with scoliosis [22]. In a study among 1030 scoliosis patients, a 1.8-fold incidence of breast cancer was observed [23]. In another study involving 5466 scoliosis patients, the breast cancer deaths were 77, which was significantly higher than the number (45.6) in the general population [22]. The radiographic diagnosis for patients of AIS was also reported to contribute to the risk of developing lung cancer up to 7.5% [24]. In addition, the cumulative radiation dose in regular X-ray examinations was found to significantly increase the risk of cancer [22]. To reduce the radiation dose, a slot-scanning radiograph system, named EOS, has been developed [25]. It was demonstrated that this system could preserve the image quality with a significant decrease in ionizing radiation [26,27]. However, the EOS system is large and expensive thus there is still a long way to go before it can be widely used in routine diagnosis. Apart from the problem of radiation, another important drawback is the large intra-operator and inter-operator variation in Cobb angle measurement, which can be up to 3–5° and 6–9° respectively [28–30]. In clinics, a curve progression is diagnosed when an increase of 5° or more is found in Cobb angle measurement [29,31]. Therefore, the large measurement variation would compromise assessment reliability and evaluation efficacy of radiographic examination, especially for long-term monitoring of scoliosis.

Compared with X-ray measurement methods, ultrasound is real-time, low-cost and radiation-free. Therefore, over the past decade, the study of evaluating scoliosis using ultrasound has been a topic of increasing attention. Recently, freehand 3-D ultrasound, allowing viewing body anatomy in 3-D space, has been advanced by combining conventional 1-D array ultrasound probe with position sensor [32–36], and a number of such systems have been developed dedicated for scoliosis evaluation. One method is to manually mark the transverse processes in 2-D ultrasound images with 3-D positional data. The target images were acquired in real-time through observations [37] or selected from the acquired 2-D image set [38]. However, this method is relatively time-consuming because each sonographic landmark has to been identified from dozens of B-mode images. Moreover, this approach generates a virtual model using the marked points instead of the 3-D ultrasound representation of the spine anatomy. Another method is to form the coronal spine image using

different visualization methods including the maximum intensity projection method [6,39] and the volume projection imaging (VPI) method [40]. In the method of the maximum intensity projection, the hyperechoic appearance of spinous processes was used to identify the spine deformity. To obtain the spinous processes images, the operator firstly manually marked the reconstruction range of the raw images and then rendered to get the coronal images [41]. Such manual procedure can reduce the influence of the surrounding tissues such as muscle. Compared with the above maximum intensity projection method, another study conducted by Cheung et al. [40] could provide the coronal image without the manual marking procedure. The principle of this study was to generate the ultrasound spine image using the shadow below the spinous processes on 2-D raw images. On the basis of the captured data sequence, a 3-D spine volume was firstly reconstructed. The coronal images were then obtained from the 3-D volume [40]. In this method, the raw image data set was usually very large (about 2,000 images, 640 × 480 pixels, about 600 MB) to cover the whole spine area. Therefore, the volume reconstruction procedure was relatively time-consuming so that the patient could not get the spine measurement report immediately after the scanning. Therefore, it is desirable to develop an ultrasound system which can provide coronal images of the spine to patients immediately after the scanning.

Accordingly, this study aims to develop a fast 3-D ultrasound projection imaging (FUPI) method for assessment of scoliosis. The shadow below the spinous processes within the acquired 2D ultrasound images were used to generate the coronal images and measure the spinal curvature. In the following sections, this system is described in details. The system repeatability was tested among the recruited scoliosis patients. The processing time and curvature measurement results of this FUPI method were compared with those by the conventional VPI method.

2. Methods

2.1. System overview

A freehand 3-D ultrasound imaging system for the assessment of scoliosis, named as Scolioscan system, was developed with ergonomic and industrial designs of the hardware. Figure 1a illustrates the system components. A rigid frame, with four supporters, the movable hip and chest boards, was designed to facilitate the patient to keep a stable posture in the examination. The operator moved the two boards along the side panel and fixed it according to the patient's height when he/she stood on the platform. The lengths of the supporters on the hip board and chest board were adjusted to align with the bilateral anterior superior iliac spines and the clavicle anterior concavities, respectively. Figure 1b shows a subject standing in front of the system with the requested stable posture. A custom-designed liner 2-D ultrasound probe (width: 10 cm; frequency: 4–10 MHz) was adopted to acquire ultrasound images. An electromagnetic spatial sensing device (driveBAY, Ascension Technology Corporation, Burlington, USA) was used to track positional data of ultrasound images. The sensor of this device was installed inside the ultrasound probe. A transmitter box was designed to hold the transmitter of the spatial device, also shown in Figure 1a. The Scolioscan system contains two LCD monitors. The information for the patient was provided by the patient monitor. During scanning, a green eye spot was displayed on the monitor according to the height of the patient to help to maintain the neck and head in a stable posture. The operator used the operator monitor to set the

system parameter, input the patient information, control the image rendering, measure the spine deformity angle, and generate reports.

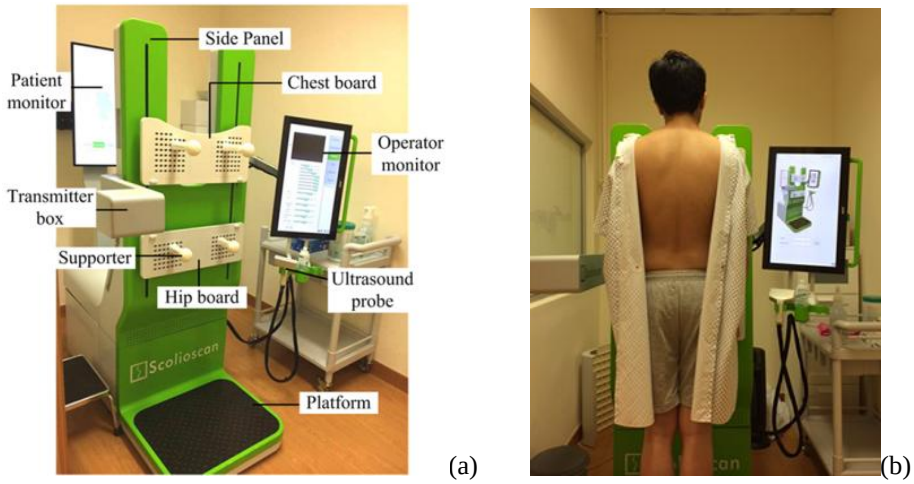

Figure 1. The 3-D freehand ultrasound imaging system for scoliosis, named Scolioscan system. (a) The system components, which mainly consist of a rigid frame, an ultrasound scanner, a position sensing device, and a computer. (b) A subject standing in front of the system in the posture as requested.

2.2. Data acquisition and fast projection imaging method

Before the ultrasound examination, all metallic items of the subject were asked to be removed to avoid the influence on the electromagnetic spatial device. The subject stood on the platform in the required posture and wore a gown with back opened to the operator. The hip board, chest board, and four supporters were adjusted by the operator to maintain the subject in the required posture. After applying suitable ultrasound gel to the spine area, the operator held the probe on the subject's back to set the system parameters, such as depth and frequency of ultrasound. In this study, the spine area from the first thoracic vertebra (T1) to the fifth lumbar vertebra (L5) was covered in the scanning. The probe was put on T1 and L5 to register the upper and lower points of the scanning, respectively. Then the probe was moved to L5 to start the scanning. Finally, the operator steered the probe to cover the spine area vertically. During scanning, ultrasound images and spatial data were captured to the computer. The collection of the data would be automatically stopped when the probe came to the recorded upper point. The whole scanning usually took about 30 seconds and about 2000 2-D ultrasound images and their corresponding spatial data were recorded for further processing.

In an earlier reported 3-D ultrasound rendering method for scoliosis assessment, namely volume projection imaging (VPI) method, two steps were used to get the spine coronal images [40]. The first step was to reconstruct to get the 3-D spine volume based on the B-mode ultrasound images and their corresponding spatial data. Then the volume was projected to visualize the coronal image. The two-step rendering method is the conventional typical 3-D ultrasound imaging method. However, the purpose of the 3-D ultrasound imaging system is to obtain the coronal or sagittal images of the spine to further assess the scoliosis. Therefore, the first step of the spine volume reconstruction in the above rendering method is not necessary. In the presented study, we proposed a fast 3-D ultrasound

projection imaging (FUPI) method to provide volume projection images. In this method, the step of volume formation was bypassed to improve the visualization speed. The rendering method, also called narrow-band volume rendering, was first introduced by Gee et al. [42,43]. The principle of the rendering method was to endow the coronal image with a certain thickness based on the raw image data and the narrow-band meant a layer with limited thickness. The developed FUPI method included three steps: Image reslicing, interpolation and image enhancement. The common reslicing method is to define a planar plane in Cartesian coordinate system and project images on this plane, as shown in Figure 2a. However, this method is not suitable to the spine imaging because the spine has a certain natural curve instead of a vertical line. The planar layers in different depths can only get a part of the spine information. To get an image which can display the spine curvature, the information of the whole spine on raw image data should be included into coronal images. Figure 2b reveals the proposed non-planar reslicing method. The left image in Figure 2b is the raw image stack in 3-D space. The spine curve was marked in black, which is roughly parallel to the skin. Therefore, the developed non-planar reslicing method used the skin as the reference to define the non-planar reslicing layer. As shown in the middle image of Figure 2b, a layer which has a certain thickness and the same distance to the skin surface was cut from the raw data set. The layer thickness was set to 3.7 mm. To cover the whole spine region, five layers along the depth were selected for each data set. The distance of the first layer to skin was set to 8.8 mm and the distance between two layers was 2.2 mm. Finally, the data of the selected layer was projected to the coronal plane to generate the spine image. To get the coronal image, a coordinate system with the regular pixel array was defined. The resolution of the pixel array was determined by the operator. On the basis of the calibration matrix and the positional data, each pixel on the non-planar layer was transformed to the defined coordinate system. On the new coronal plane, the final pixel value of the projected image was determined by averaging all pixels falling into its region. After the imaging reslicing, the second step was interpolation because of the gaps in the projected images. Many interpolation methods, such as linear interpolation, nearest neighbor interpolation, and the distance weighted interpolation, have been reported for the gap filling [44]. The common bilinear interpolation approach was implemented in this study to produce the trade-off between the interpolation performance and the computation time [33]. The empty pixel was set to the mean value of the non-empty pixels in the nearest 2-by-2 neighborhood. The third step was to enhance the image contrast. The Histogram equalization [45], a useful image enhancement method, was adopted in this study. As shown in Figure 3, the image contrast was greatly enhanced and the details were better delineated after enhancement.

To assess the spine deformity, Cheung et al. [40] developed an angle assessment approach based on coronal shadow images produced by the spinous processes. In this method, the inflection point of the spinous shadow was identified by the operator and the vertebrae including the inflection point was regarded as the most tilted one. In a spine coronal image, such as Figure 3b, the operator firstly marked short lines covering the corresponding vertebra body in the middle of the shadow curve to denote the inflection point. Then the angle was calculated between the two lines to indicate the spine curvature.

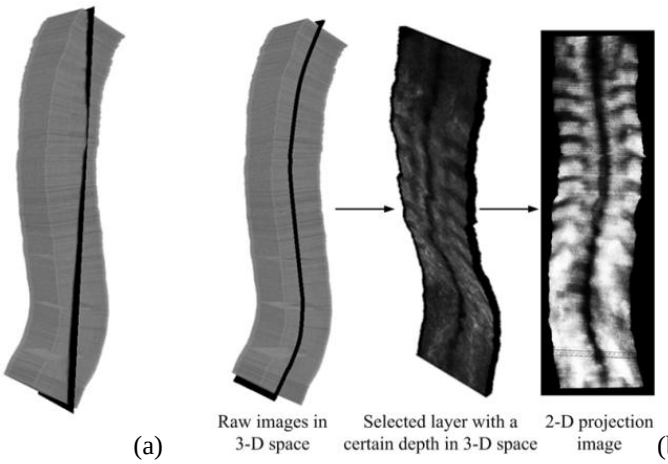

Figure 2. The planar and non-planar reslicing method. (a) The illustration of the planar reslicing approach. (b) The illustration of the non-planar reslicing approach using the skin as the reference.

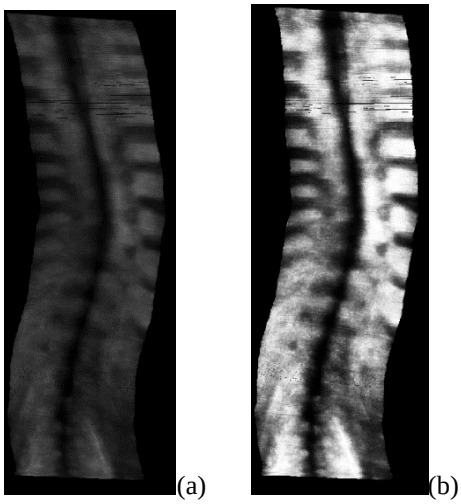

Figure 3. The projected images without enhancement and after enhancement. (a) The image without enhancement. (b) The image with enhancement.

2.3. Subjects

Formal ethics committee approval was obtained for this study. All participants (or parents for the participants under 18 years old) provided written informed consent for participation in the study. During Aug 2013 to Jul 2014, 70 patients (average age, 15.6 years ± 2.8 [standard deviation]; BMI, 18.5 ± 2.1 kg/m^2; 18 male and 52 female) who were diagnosed with scoliosis were recruited in The Chinese University of Hong Kong. The exclusion criteria were: (1) patients with metallic implants; (2) patients who had received brace or surgical treatment; (3) patients with BMI index higher than 25.0 kg/m^2. This study included two tests, the repeatability test and the performance comparison study. 20 of the recruited subjects (average age, 16.4 years ± 2.7 [standard deviation]; BMI, 18.6 ±

1.6 kg/m^2; 4 male and 16 female;) participated in the first stage of repeatability test, while all the subjects participated in the performance comparison study.

2.4. Repeatability test

To investigate the system repeatability, the intra- and inter-operator tests were performed. In the intra-operator test, each subject was scanned twice by the same operator using the Scolioscan system. For the inter-operator assessment, the second operator scanned the subject and the result was compared with the first data set of the intra-operator test. Before each scanning, the preparatory procedures, including the subject posture adjustment using the boards and supporters, and the ultrasound parameters setting, were all performed by the operator. When one scanning was completed, the subject was asked to leave the standing position and relax for about five minutes. After all the subjects were scanned, the raw data was processed and the coronal images were obtained using the newly developed projection method. For each acquired data set of the patient, five coronal images in different depths were obtained because five layers were used in the projection method as mentioned earlier. An operator investigated the five images and chose one image which could clearly demonstrate the spine curve as the measurement image. For each patient, three data sets were acquired. For the three data sets, the operator chose the image in the same depth as the measurement image to avoid the error caused by the different depths. Based on the measurement images, the other operator measured the angles using the spinous profile.

2.5. Comparison study between FUPI method and conventional VPI method

The comparison experiment was performed between the developed FUPI method and the conventional VPI method to analyze the performance of the new projection imaging method. The two imaging systems ran on the same computer with 32.0 GB of memories and configuration of Intel Core i5. 70 scoliosis patients were involved in this study. In the experiment, the patient was asked to stand on the platform of the Scolioscan system in the required posture. Then an operator held the ultrasound probe and scanned from L5 to T1. The raw data were acquired and saved in the computer. Finally the raw data including the images and their corresponding spatial data were processed by the two imaging approaches respectively. Both the processing time and the angle measurement result were compared between the two methods. To facilitate the comparison, the same reslicing parameters were used to generate the coronal images by the two imaging methods. For each patient, two image sets were obtained using the two methods. An operator reviewed the two sets and chose one image from each set which could clearly demonstrate the spine deformity as the measurement images. Then the angles were measured by the operator. 140 images (70 subjects $\times$ 2 imaging methods) were in total measured in the comparison experiment. The processing times of two imaging methods were also recorded for comparison.

2.6. Data analysis

To assess the system reproducibility, the intraclass correlation coefficient (ICC) values were calculated for intra- and inter-operator tests. For the comparison study, the processing times used by the two imaging methods on the 70 subjects were compared using the student's t-test, and a P value

of less than 0.05 was considered to indicate a significant difference. The relationship between the numbers of the raw images and the processing time was also analyzed. The spine deformity angles were manually measured on projected coronal images. The measurement results were used to compare the differences between images generated by two different rendering methods. The Pearson correlation coefficient r was calculated to evaluate the correlation of the two methods. All statistical analyses were performed using the statistical software (SPSS for Windows, version 17.0; SPSS, Chicago, IL, USA).

3. Results

3.1. Repeatability test

The intra- and inter-operator assessment results on angle measurement were summarized in Table 1. There were totally 29 angles (20.7 ± 7.5 degrees, range: 5.0–37.1 degrees). The absolute differences between the angles obtained from two scans were 1.8 ± 1.4 degrees and 2.8 ± 2.4 degrees for intra- and inter-operator test, respectively. Very good reliability of the developed method was found with ICC values of 0.96 for intra-operator test and 0.90 for inter-operator test.

Table 1. The summary of measurement angles in intra- and inter-operator tests.

	Angles (degree)
Angle number	29
Average ± SD*	20.7 ± 7.5
Range	5.0–37.1
Absolute difference for intra-operator test	1.8 ± 1.4
Absolute difference for inter-operator test	2.8 ± 2.4

3.2. Processing time comparison

The student's t-test result demonstrated a significant difference ($p < 0.001$) in the processing time of the two imaging methods. The average processing time of the developed FUPI method was 15.07 ± 0.03 s (range: 15.01–15.15 s), while the conventional VPI method took 130.31 ± 35.07 s (range: 68.30–248.59s). The processing time of the earlier method was, on average, 9 times of that spent by the new method. Moreover, the standard deviation (SD) value of the conventional VPI method was as large as 35.07 s, which reveals that the processing time varied largely among different patients. To further demonstrate this result, the relationships of the data size and the processing time for the two imaging methods were given in Figure 4. Figure 4a is for the VPI method, which presents a linear correlation between the numbers of the raw images and the processing time. While for the new FUPI method (Figure 4b), there was no such correlation. The two different correlations suggested that the processing time of the VPI method was greatly affected by the size of the raw data, while that of FUPI almost kept a constant value for different data. This feature was important for processing the large data set. For example, in this experiment, the VPI method took 248.59 s to process a data set with about 4000 raw 2D images. For the FUPI method, it only took 15.15 s to complete the rendering.

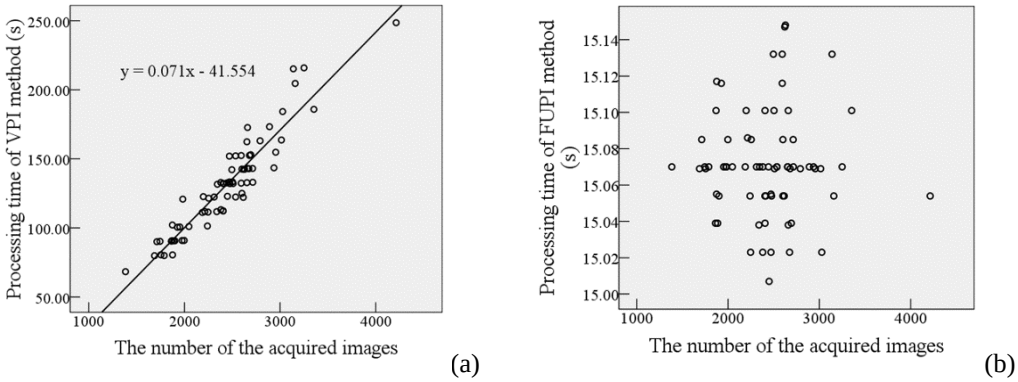

Figure 4. The relationship between the number of the acquired image and the processing time. (a) The relationship for the conventional 3-D rendering method. (b) The relationship for the new projection method.

3.3. The comparison results of the angle measurement

There were two measurement images for each subject, which were produced using the two imaging methods. Figure 5 present two typical images from the same subject using the two imaging methods, the left from VPI method and the right from the FUPI. The two images showed similar spinous and shadow features, except that the right image generated by the new projection method was shaper than the left one and showed more details. The angle measurement results using the two methods on 70 subjects were summarized in Table 2. There were totally 113 angles (19.0 ± 7.4 degrees, range: 3.4–39.5 degrees). The mean absolute difference between the results of the two methods was about 1.8 degrees. The correlation between the two measurements is shown in Figure 6a. The Bland-Altman plot (Figure 6b) showed a low mean difference (D = 0.1) and the differences symmetrically distributed around the mean difference. The measurement results of images generated by FUPI method had a very good correlation with that of the VPI method (y = 0.984x, r = 0.954). Therefore, the developed method had similar ability to the conventional imaging method in illustrating the spine deformity.

Table 2. The summary of measurement angles in the comparison study.

	angles (degree)
Angle number	113
Average ± SD	19.0 ± 7.4
Range	3.4–39.5
Difference between two measurements	1.8 ± 1.4

(a) (b)

Figure 5. The typical comparison images from the two imaging methods for the same subject. (a) The image generated by the VPI method. (b) The image formed by the new FUPI method.

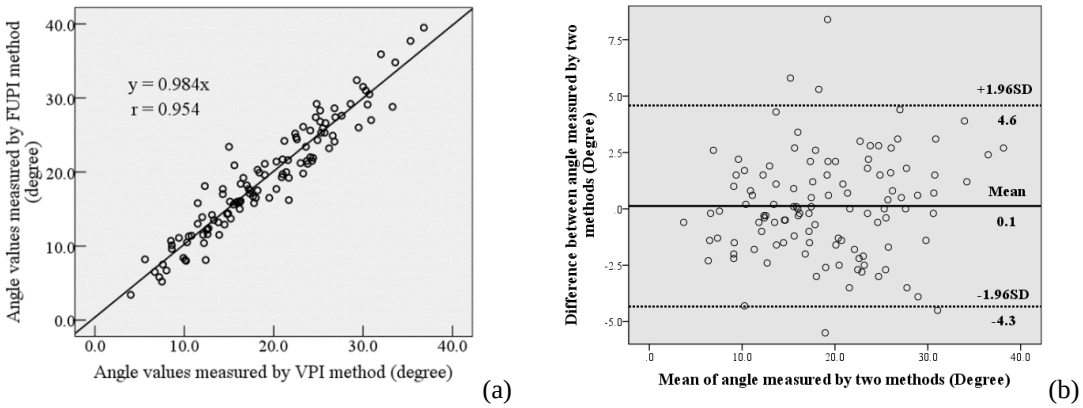

(a) (b)

Figure 6. The comparison between images generated by the developed FUPI method and the conventional VPI method. (a) The correlation of the angle measurement results. (b) Bland-Altman plot between two methods.

4. Discussion

In this study, a fast 3-D ultrasound projection imaging method for scoliosis evaluation has been presented based on the freehand ultrasound and magnetic position sensor. The intra- and inter-operator tests on scoliosis patients revealed the good repeatability of this system. Unlike the conventional 3-D volume reconstruction imaging method, this method generated the coronal image directly from the raw data set instead of from the reconstructed spine volume. The comparison test on 70 patients verified that the developed method could greatly save the processing time while preserving the comparative performance in the produced projection images, which was consistent with that reported in a preliminary study with a smaller subject number [46].

The developed FUPI method has the advantage of being time-saving. The processing time could be reduced, on average, as much as 9 times in comparison with the earlier reported 3-D reconstruction imaging method. Such feature can benefit the clinical diagnosis using the Scolioscan system. The imaging time of about 15s allows the clinician to obtain coronal images right after the scanning. If problems are found on projection images, such as a missed region in the scanning, the clinician can perform the scanning again immediately. With the short imaging time, the patients can obtain the deformity measurement results immediately after the scanning is over, which can also decrease the waiting time of patients. In addition, as shown in Figure 4, the processing time of this method did not change with the size of the acquired image data. This is very useful when large area scanning is required such as spine. In small region scanning such as finger, typical raw data ranging from 16 MB to 96 MB (about 256 scans) are acquired for the processing [33,47]. However, for the spine imaging, the data can be as much as 1 GB (more than 4000 scans) to cover the whole region. Therefore, the fixed processing time makes this projection method more suitable for large organ imaging.

In this projection method, a non-planar reslicing method was used to visualize the image of the hidden bony features inside the spine. Compared with the non-planar reslicing method, the planar reslicing method is more widely used in 3-D ultrasound imaging because of its simple implementation [48]. The planar reslicing method is to project the image according to a specific planar plane in Cartesian coordinate system, as shown in Figure 2a. However, in this study, absent regions at the spine curvature were observed if the image was processed using the planar reslicing method as marked in Figure 7. Thus the spine anatomy could not be completely displayed on the projection image. Therefore, the non-planar reslicing method was adopted in this study to help generate the projection image following the natural curve of the spine so as to provide a better visualization of the spine features.

Figure 7. The projection image processed using the planar reslicing method. The absent region was marked.

Although the newly proposed approach achieved obvious advantages over previous methods for clinical scoliosis assessment, there are limitations to be overcome in future studies. One limitation is

that the skin was used as the reference to get the projection layer in implementation of the non-planar reslicing. As shown in Figure 2b, the purpose of the reslicing method was to project the layer which contains the spine information to the plane of the projection image. In this study, to simplify the layer definition procedure, the skin was used as the reference and the layer which had the same distance to the skin was chosen to project to generate the image. However, the spine is not always parallel to the skin because the muscle thickness is different in different regions of the back. So the vertebra may not be divided into the same layer in this method. One approach to solve this problem is to manually mark the spinous process on the 2-D raw images. Then the layer containing the marked regions can be projected to generate the coronal images. Another limitation of this method is that five coronal images from different layers were generated and one image was chosen from the five images as the measurement image. So the angle measurement result represents the angle in a certain depth. However, there may be different measurement angles in different depths of the spine. In the future study, the measurement angles in different depths and their average value will be compared to find an angle to represent the spine curvature.

Despite these limitations, our results suggested that the developed method has the potential to provide fast and reliable 3-D ultrasound imaging for scoliosis. In fact, this method provides the projection image based on the hyperechoic appearance of the bone within the acquired 2-D ultrasound images, thus it is expected to be used in more fields to image the bones such as the thoracic paravertebral space [49], femur volume [50], and the hand and wrist joints [51].

5. Conclusions

The present study demonstrated a fast 3-D ultrasound projection imaging method for scoliosis evaluation. The system repeatability was very good. The comparison study demonstrated that the developed method could greatly save the processing time while preserving the comparative ability in illustrating the spine deformity. It can be expected that this novel method may help to provide fast and effective 3-D ultrasound examination of scoliosis in clinics. In addition, with the advancement of this method, the fast 3-D ultrasound system has potential to be used for imaging other bones.

Acknowledgements

This study was supported by the National Natural Science Foundation of China (61701442, 61771130), the Research Grant Council of Hong Kong (PolyU5332/07E, PolyU152220/14E), the Hong Kong Innovation and Technology Fund (UIM213), the Natural Science Foundation of Zhejiang Province (LY18F030019) and the Natural Science Foundation of Guangdong Province (2015A030310268). The authors would like to thank the generous supports from staff of Telefield Medical Imaging Limited for providing the Scolioscan system and technical supports for this study. Thanks are also given to Prof. Jack Chun-Yiu Cheng and Dr. Tsz-Ping Lam of The Chinese University of Hong Kong for their help in recruiting subjects and patients who participated in this study. Thanks are also given to S. Ding for her editing of the manuscript.

Conflict of interest

The authors declare no competing interests.

References

1. T. Hattori, H. Sakaura, M. Iwasaki, Y. Nagamoto, H. Yoshikawa and K. Sugamoto, In vivo three-dimensional segmental analysis of adolescent idiopathic scoliosis, *Eur. Spine J.*, **20** (2011), 1745–1750.
2. M. H. Pope, I. A. Stokes and M. Moreland, The biomechanics of scoliosis, *Crit. Rev. Biomed. Eng.*, **11** (1984), 157–188.
3. S. P. Tang, J. C. Y. Cheng and T. P. Lam, Adolescent Idiopathic Scoliosis (AIS): An overview of the etiology and basic management principles, *HK. J. Paediatr.*, **8** (2003), 299–306.
4. J. P. Horne, R. Flannery and S. Usman, Adolescent Idiopathic Scoliosis: Diagnosis and management, *Am. Fam. Physician.*, **89** (2014), 193–198.
5. M. Konieczny, H. Senyurt and R. Krauspe, Epidemiology of adolescent idiopathic scoliosis, *J. Child.*, **7** (2013), 3–9.
6. E. Lou, A. Chan, A. Donauer, M. Tilburn and D. Hill, Ultrasound-assisted brace casting for adolescent idiopathic scoliosis, *Scoliosis.*, **10** (2015), 1–6.
7. S. L. Weinstein, L. A. Dolan, K. F. Spratt, K. K. Peterson, M. J. Spoonamore and I. V. Ponseti, Health and function of patients with untreated idiopathic scoliosis: A 50-year natural history study, *JAMA.*, **289** (2003), 559–567.
8. J. Theroux, S. Le May, C. Fortin and H. Labelle, Prevalence and management of back pain in adolescent idiopathic scoliosis patients: A retrospective study, *Pain. Res. Manag.*, **20** (2015), 153–157.
9. R. M. Campbell, M. D. Smith, T. C. Mayes, J. A. Mangos, D. B. Willey-Courand, N. Kose, R. F. Pinero, M. E. Alder, H. L. Duong and J. L. Surber, The characteristics of thoracic insufficiency syndrome associated with fused ribs and congenital scoliosis, *J. Bone. Joint. Surg. Am.*, **85A** (2003), 399–408.
10. P. R. P. Rushton and M. P. Grevitt, Comparison of untreated adolescent idiopathic scoliosis with normal controls: A review and statistical analysis of the literature, *Spine*, **38** (2013), 778–785.
11. M. de Seze and E. Cugy, Pathogenesis of idiopathic scoliosis: A review, *Ann. Phys. Rehabil. Med.*, **55** (2012), 128–138.
12. Y. Zhang, Y. J. Yang, X. Q. Dang, L. Zhao, J. Ren, L. G. Zhang and J. Z. Sun, Factors relating to curve progression in female patients with adolescent idiopathic scoliosis treated with a brace, *Eur. Spine J.*, **24** (2015), 244–248.
13. S. Hoppenfeld, B. Lonner, V. Murthy and Y. Gu, The rib epiphysis and other growth centers as indicators of the end of spinal growth, *Spine*, **29** (2004), 47–50.
14. H. F. Wu, J. L. Ronsky, F. Cheriet, J. Harder, J. C. Kupper and R. F. Zernicke, Time series spinal radiographs as prognostic factors for scoliosis and progression of spinal deformities, *Eur. Spine J.*, **20** (2011), 112–117.
15. M. Thomsen and R. Abel, Imaging in scoliosis from the orthopaedic surgeon's point of view, *Eur. J. Radiol.*, **58** (2006), 41–47.
16. H. Kim, H. S. Kim, E. S. Moon, C. S. Yoon, T. S. Chung, H. T. Song, J. S. Suh, Y. H. Lee and S. Kim, Scoliosis imaging: What radiologists should know, *Radiographics*, **35** (2015), 1.
17. B. V. Reamy and J. B. Slakey, Adolescent idiopathic scoliosis: Review and current concepts, *Am. Fam. Physician.*, **64** (2001), 111–116.

18. S. D. Glassman, L. Y. Carreon, C. I. Shaffrey, D. W. Polly, S. L. Ondra, S. H. Berven and K. H. Bridwell, The costs and benefits of nonoperative management for adult scoliosis, *Spine,* **35** (2010), 578–582.
19. S. L. Weinstein, L. A. Dolan, J. G. Wright and M. B. Dobbs, Effects of bracing in adolescents with idiopathic scoliosis, *N. Engl. J. Med.*, **369** (2013), 1512–1521.
20. E. J. Carragee and R.A. Lehman, Spinal bracing in adolescent idiopathic scoliosis, *N. Engl. J. Med.*, **369** (2013), 1558–1560.
21. J. Cobb, Outline for the study of scoliosis, *Am. Aca. Ortho. Surgeon. Instruct. Course Lect.*, **5** (1948), 15.
22. M. M. Doody, J. E. Lonstein, M. Stovall, D. G. Hacker, N. Luckyanov and C. E. Land, Breast cancer mortality after diagnostic radiography: Findings from the US scoliosis cohort study, *Spine*, **25** (2000), 2052–2063.
23. D. A. Hoffman, J. E. Lonstein, M. M. Morin, W. Visscher, B. S. Harris and Jr J.D. Boice, Breast cancer in women with scoliosis exposed to multiple diagnostic X-rays, *J. Natl. Cancer*, **81** (1989), 1307–1312.
24. C. L. Nash, E. C. Gregg, R. H. Brown and K. Pillai, Risks of exposure to X-rays in patients undergoing long-term treatment for scoliosis, *J. Bone. Joint. Surg. Am.*, **61** (1979), 371–374.
25. G. Kalifa, Y. Charpak, C. Maccia, E. Fery-Lemonnier, J. Bloch, J. M. Boussard, M. Attal, J. Dubousset and C. Adamsbaum, Evaluation of a new low-dose digital X-ray device: First dosimetric and clinical results in children, *Pediatr. Radiol.*, **28** (1998), 557–561.
26. Z. Al-Aubaidi, D. Lebel, K. Oudjhane and R. Zeller, Three-dimensional imaging of the spine using the EOS system: Is it reliable? A comparative study using computed tomography imaging, *J. Pediatr. Orthop. Part. B.*, **22** (2013), 409–412.
27. S. Deschenes, G. Charron, G. Beaudoin, H. Labelle, J. Dubois, M. C. Miron and S. Parent, Diagnostic imaging of spinal deformities reducing patients radiation dose with a new slot-scanning X-ray imager, *Spine*, **35** (2010), 989–994.
28. D.L. Carman, R.H. Browne and J.G. Birch, Measurement of scoliosis and kyphosis radiographs. Intraobserver and interobserver variation, *J. Bone. Joint. Surg. Am.*, **72A** (1990), 328–333.
29. J. Pruijs, M. Hageman, W. Keessen, R. Vandermeer, R. Vanwieringen and J.C. Vanwieringen, Variation in Cobb angle measurements in scoliosis, *Skeletal. Radiol.*, **23** (1994), 4.
30. W. P. Bunnell, The natural history of idiopathic scoliosis before skeletal maturity, *Spine,* **11** (1986), 773–776.
31. Q. H. Huang, J. L. Lan and X. L. Li, Robotic arm based automatic ultrasound scanning for three-dimensional imaging, *IEEE. T. Ind. Inform.*
32. W. W. Jiang, C. Li, A. H. Li and Y. P. Zheng, A novel breast ultrasound system for providing coronal images: System development and feasibility study, *Ultrasonics.*, **56** (2015), 427–434.
33. Q. H. Huang, B. W. Wu, J. L. Lan and X. L. Li, Fully automatic three-dimensional ultrasound imaging based on conventional B-scan, *IEEE. T. Biomed. Circ. Syst.*, **12** (2018), 426–436.
34. Q. H. Huang, Z. Z. Zeng and X. L. Li, 2.5-Dimensional Extended Field-of-View Ultrasound, *IEEE. T. Med. Imaging*, **37** (2018), 851–859.
35. Q. H. Huang and Z. Z. Zeng, A review on real-time 3D ultrasound imaging technology, *Biomed. Res. Int.*, **2017** (2017), 20.

36. T. Ungi, F. King, M. Kempston, Z. Keri, A. Lasso, P. Mousavi, J. Rudan, D. P. Borschneck and G. Fichtinger, Spinal curvature measurement by tracked ultrasound snapshots, *Ultras. Med. Biol.*, **40** (2014), 447–454.
37. C. W. J. Cheung, G. Q. Zhou, S. Y. Law, K. L. Lai, W. W. Jiang and Y. P. Zheng, Freehand three-dimensional ultrasound system for assessment of scoliosis, *J. Orthop. Transl.*, **3** (2015), 123–133.
38. M. Young, D. L. Hill, R. Zheng and E. Lou, Reliability and accuracy of ultrasound measurements with and without the aid of previous radiographs in adolescent idiopathic scoliosis (AIS), *Eur. Spine J.*, **24** (2015), 1427–1433.
39. C. W. J. Cheung, G. Q. Zhou, S. Y. Law, T. M. Mak, K. L. Lai and Y. P. Zheng, Ultrasound volume projection imaging for assessment of scoliosis, *IEEE. T. Med. Imaging*, **34** (2015), 1760–1768.
40. W. Chen, E. M. Lou, P. Zhang, Q. Phoebe, H. L. Lawrence and D. Hill, Reliability of assessing the coronal curvature of children with scoliosis by using ultrasound images, *J. Child. Orthop.*, **7** (2013), 521–529.
41. R. W. Prager, A. Gee and L. Berman, Stradx: Real-time acquisition and visualization of freehand three-dimensional ultrasound, *Med. Image. Anal.*, **3** (1999), 129–140.
42. A. Gee, R. Prager, G. Treece and L. Berman, Narrow-band volume rendering for freehand 3D ultrasound, *Comput. Graph-UK.*, **26** (2002), 463–476.
43. Q. H. Huang and Y. P. Zheng, An adaptive squared-distance-weighted interpolation for volume reconstruction in 3D freehand ultrasound, *Ultrasonics*, **44** (2006), E73–E77.
44. E. Yeom, K. H. Nam, D. G. Paeng and S. J. Lee, Improvement of ultrasound speckle image velocimetry using image enhancement techniques, *Ultrasonics.*, **54** (2014), 205–216.
45. W. W. Jiang, G. Q. Zhou, K. L. Lai and Y. P. Zheng, Quantitative evaluation of spinal coronal curvature for scoliosis using a fast 3-D Ultrasound projection imaging method, *Int. Confer. In. Biomed. Eng. Life Sci.*, **56** (2015), 313–317.
46. M. Hünerbein, M. Raschke, C. Khodadadyan, P. Hohenberger, N. P. Haas and P. M. Schlag, Three-dimensional ultrasonography of bone and soft tissue lesions, *Eur. J. Ultras.*, **13** (2001), 17–23.
47. K. D. Kalache, K. Eder, T. Esser, H. Proquitte, G. Stoltenburg-Didinger, J. P. Hartung and C. Bamberg, Three-dimensional ultrasonographic reslicing of the fetal brain to assist prenatal diagnosis of central nervous system anomalies, *J. Ultras. Med.*, **25** (2006), 509–514.
48. M. K. Karmakar, X. Li, J. W. Li and A. Hadzic, Volumetric three-dimensional ultrasound imaging of the anatomy relevant for thoracic paravertebral block, *Anesth. Analg.*, **115** (2012), 1246–1250.
49. C. Ioannou, I. Sarris, R. Napolitano, E. Ohuma, M. K. Javaid and A. T. Papageorghiou, A longitudinal study of normal fetal femur volume, *Prenatal. Diag.*, **33** (2013), 1088–1094.
50. G. Peluso, S. L. Bosello, E. Gremese, L. Mirone, F. Di Gregorio, V. Di Molfetta, T. Pirronti and G. Ferraccioli, Detection of bone erosions in early rheumatoid arthritis: 3D ultrasonography versus computed tomography, *Clin. Rheumatol.*, **34** (2015), 1181–1186.

AIMS Press